Idealised Ocean Modelling

T.D.J du Val de Beaulieu
CID: 00927945
Word count: 5987

08th May, 2017

Abstract

The LPS model was developed in 1983 and predicts the depth of the density layers in ocean due to forcing from the wind. The model uses three discrete density layers in motion. The solution to this model was compared to observational data from the Argo project to find out if it correctly fitted the ocean. Initially, the model did not produce a close fit to the density layers; therefore, different aspects of the model were changed to improve its accuracy. The most significant was the choice of density layers which provided a significant improvement to the solution. The solution to the North Atlantic and North Pacific Ocean were found and compared, where the model predicted the North Pacific better due its more rectangular shape and larger size.

Contents

List of Figures

Chapter 1

Introduction

The motion within the first two kilometers of the ocean was studied in great detail in the 1980s [1]. The pursuit of understanding what causes ocean circulation was highly important to furthering our knowledge of the ocean. It was understood that the wind played a significant role, driving the sea horizontally and vertically. This effect creates coupling between the ocean and the atmosphere. Two conflicting theories were developed which described this phenomenon.

The first paper was by Rhines and Young which investigated the deeper part of the ocean, considered unventilated [2]. Therefore, this region would not have been recirculated to the top of the ocean, having low oxygen content within. The paper explained that the movement can be described by the homogenization of the potential vorticity. This is a result of quasi-geostrophic flow, derived in the theory. The counter argument was written by Luyten, Pedlosky and Stommel and considered the higher ventilated region [3]. This described how the wind stress sets into motion discrete density layers of fluid. These layers are driven downwards and are subducted by new layers. Following these papers, Pedlosky and Young wrote a paper which combined the two models (PY model), analysing the discrepencies in more detail [4]. Furthermore, the LPS and PY models have been developed from discrete density layer to continuous stratification by Huang [5].

The most significant result of the LPS model was due to its strict boundary conditions which led to the derivation of the shadow zone. Within this area, a layer that could previously move became stagnant and, therefore, unventilated. The presence of the ventilated region has been analysed in detail by Talley by investigating the salinity within the North Pacific Ocean [6]. The unventilated region has been investigated by analysing oxygen levels within the ocean. Recently, the model has been used to understand the impact that global warming has on ocean ventilation [7].

The aims of this project were to program and check the LPS model. The model was then analysed and compared to observed data from the Argo project. This created a clear comparison to see whether the LPS model predicted the change in density throughout the ocean. Furthermore, parameters within the model where changed to see which had the most significant impact to the solution. The limitation of the model were discussed throughout this report as well as further investigations which could be performed to better our understanding.

Chapter 2

The LPS model

The LPS model was used to describe how density changes with depth through the oceans. The model has an arbitrarily large number of inviscid, homogeneous and immiscible fluid layers. Each layer has a discrete density with the density increasing with depth. For this project, four layers were used where three of these layers were in motion. The model does not depend on time.

2.1 Notation

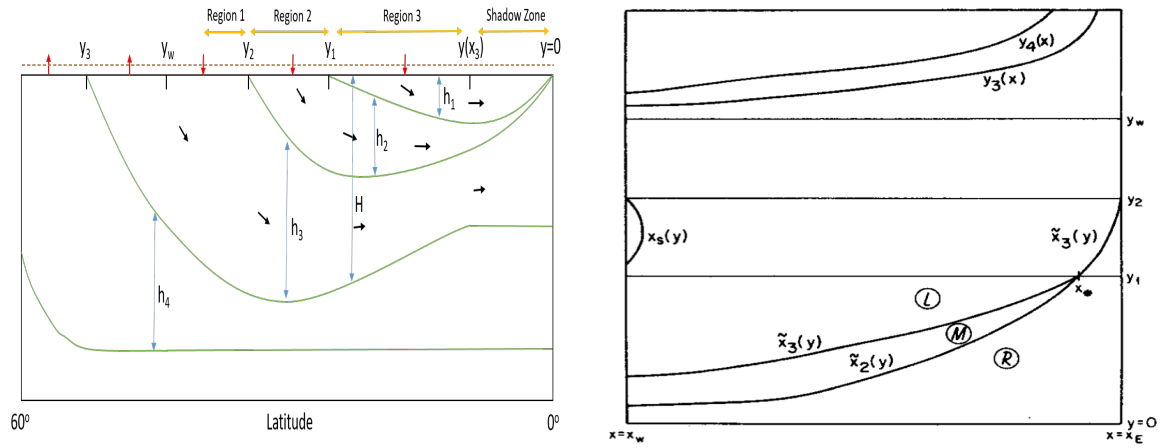

(a) Cross-section

(b) Plane view

Figure 2.1: (a) shows a sketch of the solution to the LPS model. A cross-section at a constant latitude across the ocean from 60° north until the equator. (b) shows the plane view of a sketch of the LPS solution [3]. The model is derived using a square basin.

The cross-section shows the discrete density layers moving towards the equator from the north. The dotted line is the Ekman layer and provides a downwards forcing south of y_w. The fourth layer is assumed to be motionless and, therefore, flat for $y < y_w(x)$. This means that only three layers are in motion. The term H is the depth of the bottom of layer 3. The only boundary condition is that on the eastern boundary ($x = x_E$) geostrophic zonal flow goes to zero. Note, the theory derives the solution using a Cartesian coordinate system. This can be transformed into spherical coordinates using $dx = Rcos\theta d\lambda$ and $dy = Rd\phi$, where $d\lambda$ is longitude, $d\phi$ is latitude and R is the radius of Earth.

2.2 Fundamental physics

The model is Sverdrupian. This defines the motion of each layer as geostrophic, hydrostatic and incompressible. Using these relationships, the Sverdrup vorticity equation and the Sverdrup relation can be derived. These equations can be used to describe how fluid moves while being forced downwards or upwards (Ekman pumped). If the fluid is not being Ekman pumped, they can also be used to derive the conservation of potential vorticity. This describes the motion of a layer which is not exposed to the Ekman layer.

2.2.1 Geostrophic motion

Geostrophic motion can be derived from the Navier-Stokes equation in a rotating frame [8],

$$\frac{d\vec{u}}{dt} = -\frac{1}{\rho}\nabla P - \vec{g} + \mu\nabla^2\vec{u} + \Omega^2\vec{r} - 2\vec{\Omega}\times\vec{u}. \tag{2.1}$$

The final two terms are the centrifugal and Coriolis acceleration, respectively. Now consider the Rossby number of the ocean, which is the ratio of the inertial force to the Coriolis force [9],

$$R_0 = \frac{U}{Lf} \tag{2.2}$$

where U is the velocity, L is the length scale and f is the Coriolis parameter ($2\Omega\sin\phi$). The ocean's Rossby number at mid latitudes is less than 1. This provides evidence that the inertial terms in the Navier-Stokes can be neglected. This leaves the Coriolis acceleration and the term containing the derivative of the pressure.

Rearranging the simplified Navier-Stokes equation, the geostrophic motion is defined as,

$$\rho_n f u_n = -\frac{\partial P}{\partial y} \tag{2.3a}$$

$$\rho_n f v_n = \frac{\partial P}{\partial x} \tag{2.3b}$$

where ρ is the density, P is the pressure, and u_n and v_n are the fluid speeds in the x and y direction, respectively.

2.2.2 Hydrostatic motion

Hydrostatic motion can be found by equating the vertical change in pressure to the weight of the ocean above. Using the pressure above and the density of a column of water, the equation can be found to be

$$\rho g = \frac{\partial P}{\partial z} \tag{2.4}$$

where z is in the downwards direction.

2.2.3 Incompressible motion

Incompressible motion is described by the continuity equation,

$$\frac{\partial u_n}{\partial x} + \frac{\partial v_n}{\partial y} + \frac{\partial w_n}{\partial z} = 0 \tag{2.5}$$

2.2.4 The Sverdrup vorticity equation

The Sverdrup is obtained from the hydrostatic (2.3) and incompressible (2.5) equations. The different velocity components (2.3a) and (2.3b) are differentiated again with respect to x and y, respectively. This allows the pressures to be equated. The derivation is shown in the appendix. Note that $f = f(y)$ and $\rho = \rho(z)$ when differentiating. The resulting equation is,

$$\beta v_n = -f\left(\frac{\partial u_n}{\partial x} + \frac{\partial v_n}{\partial y}\right) \tag{2.6}$$

where $\beta = \frac{df}{dy}$. Using (2.5), the Sverdrup vorticity equation can be written as

$$\beta v_n = f\frac{\partial w_n}{\partial z}. \tag{2.7}$$

The vertical movement of the water is found from Ekman pumping.

2.2.5 The Sverdrup relationship

The Sverdrup relationship is the integral of the Sverdrup vorticity equation (2.7) over all layers. As these layers are discrete, the integral can be approximated as a sum.

$$\sum_n \beta v_n h_n = f w_e(x, y) \tag{2.8}$$

The Ekman pumping is denoted by $w_e(x, y)$ which is the vertical velocity of the layer when exposed to the Ekman layer. The height of the layer is h_n.

2.2.6 Conservation of potential vorticity

Potential vorticity is an important concept in the LPS model and in oceanography. The potential vorticity ($\frac{f+\varepsilon}{h}$) is the measure of angular momentum with respect to the height of a column of water. The Rossby approximation means that it does not depend on the actual rotation (ε) but only the Coriolis parameter (f). The derivation of its conservation is beyond the scope of this project, but requires the closed material contour to be conserved [10].

If the layer is shielded from the wind by an intervening layer ($w_n = 0$), the shielded layer conserves its potential vorticity $\left(\frac{f}{h}\right)$. The conservation requires the use of the total derivative of the potential vorticity [11]; this quantity is zero when it is conserved.

$$q_n(x,y) = \frac{f(y)}{h(x,y)} \tag{2.9}$$

$$\frac{D}{Dt} = \frac{\partial}{\partial t} + u \cdot \nabla \tag{2.10}$$

Note, q_n does not depend on t and z in (2.9).

$$u_n \frac{\partial q_n}{\partial x} + v_n \frac{\partial q_n}{\partial y} = 0 \tag{2.11}$$

2.3 First region $(y_2 \leq y \leq y_w)$

The first region of the LPS only contains layers 3 and 4. Layer 4 has a trivial solution where the depth is constant at its lower interface and its velocity is constant throughout. The velocities of the third layer can be found by integrating the hydrostatic equation. The derivation is shown in the appendix. The velocities are,

$$u_3 = -\frac{\gamma_3}{f}\frac{\partial}{\partial y} h_3 \tag{2.12a}$$

$$v_3 = \frac{\gamma_3}{f}\frac{\partial}{\partial x} h_3 \tag{2.12b}$$

where $\gamma_3 = \frac{g(\rho_4 - \rho_3)}{\rho_3}$. This formula assumes that the change in density over the layer is small in comparison to the density. The approximation can be assumed to be true for the model considering typical densities within the ocean are around $1026 kgm^{-3}$ and the changes in density between layers are about $1 kgm^{-3}$. Using the Sverdrup relationship,

$$\beta \frac{\gamma_3}{f}\frac{\partial}{\partial x}(h_3)h_3 = f w_e(x,y) \tag{2.13a}$$

$$\frac{\partial}{\partial x}(h_3)h_3 = \frac{f^2}{\beta\gamma_3} w_e(x,y) \tag{2.13b}$$

$$\frac{1}{2}\frac{\partial}{\partial x}(h_3^2) = \frac{f^2}{\beta\gamma_3} w_e(x,y) \tag{2.13c}$$

$$\frac{\partial}{\partial x}(h_3^2) = \frac{2f^2}{\beta\gamma_3} w_e(x,y) \tag{2.13d}$$

The resulting equation is integrated from x to x_E, the x-coordinate of the eastern boundary.

$$h_3^2(x_E,y) - h_3^2(x,y) = \int_x^{x_E} \frac{2f^2}{\beta\gamma_3} w_e(x,y)dx \tag{2.14a}$$

$$h_3^2(x,y) = h_3^2(x_E,y) - \int_x^{x_E} \frac{2f^2}{\beta\gamma_3} w_e(x,y)dx \tag{2.14b}$$

$$h_3^2 = H_0^2 + D_0^2(x,y) \tag{2.14c}$$

$$h_3 = \left[H_0^2 + D_0^2(x,y)\right]^{\frac{1}{2}} \tag{2.14d}$$

where,

$$D_0^2 = -\int_x^{x_E} \frac{2f^2}{\beta\gamma_3} w_e(x,y)dx \tag{2.15}$$

Physically, this results in the fluid being driven down and southwards. This is a key theoretical result of the LPS model which should be observed when testing the model.

2.4 Second region $(y_1 \leq y \leq y_2)$

This region is more complex because two layers are now in motion. The lower layer (layer 3) receives no forcing from Ekman pumping, therefore this layer conserves potential vorticity. The layer above is now driven by Ekman pumping. The outcrop is where this layer originates leading to $h_2 = 0$ across this line.

The velocities for the layer 3 are adapted; the depth of the layer is denoted by $H = h_2 + h_3$. We can prove that the velocity is continuous across the boundary by setting $h_2 = 0$, thus $H = h_3$. The velocity in region 2 is,

$$u_3 = -\frac{\gamma_3}{f}\frac{\partial}{\partial y}H_3 \tag{2.16a}$$

$$v_3 = \frac{\gamma_3}{f}\frac{\partial}{\partial x}H_3 \tag{2.16b}$$

We can now invoke the equation for the conservation of potential vorticity. The potential vorticity can be denoted as $q = \frac{f}{h}$.

$$u_3\frac{\partial}{\partial x}\frac{f}{h_3} + v_3\frac{\partial}{\partial y}\frac{f}{h_3} = 0 \tag{2.17a}$$

$$u_3\frac{\partial}{\partial x}(q_3) + v_3\frac{\partial}{\partial y}(q_3) = 0 \tag{2.17b}$$

$$-\frac{\gamma_3}{f}\frac{\partial H}{\partial y}\frac{\partial q_3}{\partial x} + \frac{\gamma_3}{f}\frac{\partial H}{\partial x}\frac{\partial q_3}{\partial y} = 0 \tag{2.17c}$$

$$\frac{\partial H}{\partial x}\frac{\partial q_3}{\partial y} - \frac{\partial H}{\partial y}\frac{\partial q_3}{\partial x} = 0 \tag{2.17d}$$

The Jacobian can be used to solve the equation.

$$J(a,b) = \frac{\partial a}{\partial x}\frac{\partial b}{\partial y} - \frac{\partial b}{\partial x}\frac{\partial a}{\partial y} \tag{2.18}$$

Using an identity for the Jacobian, if $J(a,b) = 0$ then $b = G(a)$. Within the second region, $J(H, q_3) = 0$; therefore, $J(H, \frac{f}{h_3}) = 0$. This leads to $\frac{f}{h_3} = G_3(H)$. At the outcrop of the second region (y_2), $h_3 = H$ and $\frac{f_2}{H(y_2)} = G_3(H(y_2))$. Noting, $H(y_2) = H$ by equating the arguments of G_3. Therefore, the equations are continuous across the outcrop,

$$\frac{f}{h_3} = \frac{f_2}{H(y_2)} \tag{2.19a}$$

$$h_3 = \frac{f}{f_2} H(y_2) \tag{2.19b}$$

$$h_3 = \frac{f}{f_2} H \tag{2.19c}$$

This can be combined with the equation $H = h_2 + h_3$ to find a relation between h_2 and H,

$$h_2 = \left(1 - \frac{f}{f_2}\right) H \tag{2.20}$$

The velocity for layer 2 can be derived in a similar way to layer 3,

$$u_2 = -\frac{1}{f}\frac{\partial}{\partial y}\left(\gamma_3 H + \gamma_2 h_2\right) \tag{2.21a}$$

$$v_2 = \frac{1}{f}\frac{\partial}{\partial x}\left(\gamma_3 H + \gamma_2 h_2\right) \tag{2.21b}$$

The Sverdrup relationship for a two layer system can be used to find an equation for H,

$$\beta\left(h_3 v_3 + h_2 v_2\right) = f w_e(x,y) \tag{2.22a}$$

$$h_3 \frac{\gamma_3}{f}\frac{\partial H}{\partial x} + h_2 \frac{1}{f}\frac{\partial}{\partial x}(\gamma_3 H + \gamma_2 h_2) = \frac{f}{\beta} w_e(x,y) \tag{2.22b}$$

$$\gamma_3 H \frac{\partial H}{\partial x} + \gamma_2 h_2 \frac{\partial h_2}{\partial x} = \frac{f^2}{\beta} w_e(x,y) \tag{2.22c}$$

$$\frac{\partial}{\partial x}\left(H^2 + \frac{\gamma_2}{\gamma_3} h_2^2\right) = \frac{2f^2}{\beta\gamma_3} w_e(x,y) \tag{2.22d}$$

This can be integrated,

$$\left(H^2(x_E) + \frac{\gamma_2}{\gamma_3} h_2^2(x_E)\right) - \left(H^2 + \frac{\gamma_2}{\gamma_3} h_2^2\right) = \int_x^{x_E} \frac{2f^2}{\beta\gamma_3} w_e(x,y) \tag{2.23a}$$

$$H^2 + \frac{\gamma_2}{\gamma_3} h_2^2 = \left(H^2(x_E) + \frac{\gamma_2}{\gamma_3} h_2^2(x_E)\right) + D_0^2 \tag{2.23b}$$

$$H^2\left[1 + \frac{\gamma_2}{\gamma_3}\frac{h_2^2}{H^2}\right] = \left(H^2(x_E) + \frac{\gamma_2}{\gamma_3} h_2^2(x_E)\right) + D_0^2 \tag{2.23c}$$

The equation can be simplified by noting that $\frac{\gamma_2}{\gamma_3} h_2^2(x_E) = 0$. This is a result of $h_2 = 0$ on the eastern boundary from $D_0 = 0$.

$$H = \frac{\left[H_0^2 + D_0^2\right]^{\frac{1}{2}}}{\left[1 + \frac{\gamma_2}{\gamma_3}\frac{h_2^2}{H^2}\right]^{\frac{1}{2}}} \tag{2.24}$$

An equation for $\frac{h_2}{H}$ can be substituted in using (2.20).

$$H = \frac{[H_0^2 + D_0^2]^{\frac{1}{2}}}{\left[1 + \frac{\gamma_2}{\gamma_3}\left(1 - \frac{f}{f_2}\right)^2\right]^{\frac{1}{2}}} \tag{2.25}$$

The Shadow zone:

A significant property found by the strict boundary conditions, of this model, is the shadow zone. This is an area in the ocean where there are unventilated layers. This can be characterised by stating that the velocity of the fluid going into or out of the eastern boundary must be zero. This can be written as,

$$\frac{\partial H}{\partial y} = 0 \tag{2.26a}$$

$$\frac{\partial}{\partial y}\left(1 - \frac{f}{f_2}\right) = 0 \tag{2.26b}$$

The value of D_0 on the eastern boundary, by definition, is zero. The boundary condition is held if the depth of the layers (h_2 and H) stay constant when approaching the eastern boundary. This allows u_2 and u_3 to equal zero. Theoretically, if $H_0 = 0$ the depth of the water cannot decrease any further. This creates a lower bound on the values of H to $H \geq H_0$. For all depth where $H_0 \neq 0$, the same condition can still be used. The boundary at which $H = H_0$ can be found by substituting H_0 into (2.25).

$$D_0^2(\tilde{x}_3, y) = \frac{\gamma_2}{\gamma_3} H_0^2 \left(1 - \frac{f}{f_2}\right)^2 \tag{2.27}$$

South of the value of $\tilde{x}_3(y)$ found from this equation, the depth of the water decreases above H_0 which is not allowed. The line of $H = H_0$ creates a boundary. We find that this line originates from the eastern boundary at $y = y_2$; therefore, there is no potential vorticity trajectory that can ventilate layer 3. The area north of this line has two ventilated layers and south has just one. In this area, layer 3 can have the maximum allowed depth of H_0. Therefore, $H = H_0$ where $x < \tilde{x_3}$. Because the potential vorticity is no longer conserved, different equations of h_2 and h_3 are required. The equations are,

$$h_2 = \left(\frac{\gamma_3}{\gamma_2}\right)^{\frac{1}{2}} D_0(x, y) \tag{2.28a}$$

$$h_3 = H_0 - \left(\frac{\gamma_3}{\gamma_2}\right)^{\frac{1}{2}} D_0(x, y) \tag{2.28b}$$

2.5 Third region ($y \leq y_1$)

The last region that is incorporated in the model includes three layers, starting at the outcrop of layer 1. The equation for H is now adapted to include h_1: $H = h_1 + h_2 + h_3$. The velocities for each layer can be calculated using the same principle used for region 1 and 2 in the appendix,

$$v_3 = \frac{1}{f}\frac{\partial}{\partial x}\left(\gamma_3(h_1 + h_2 + h_3)\right) \tag{2.29a}$$

$$v_2 = \frac{1}{f}\frac{\partial}{\partial x}\left(\gamma_3(h_1 + h_2 + h_3) + \gamma_2(h_1 + h_2)\right) \tag{2.29b}$$

$$v_1 = \frac{1}{f}\frac{\partial}{\partial x}\left(\gamma_3(h_1 + h_2 + h_3) + \gamma_2(h_1 + h_2) + \gamma_1 h_1\right) \tag{2.29c}$$

The Sverdrup relationship can be used to find H. The same method has been implemented with the updated Sverdrup relationship and the velocities for the layers. We require a new variable, the depth of layer 2, to be defined: $I = h_1 + h_2$.

$$\beta\left(h_3 v_3 + h_2 v_2 + h_1 v_1\right) = f w_e(x, y) \tag{2.30}$$

After substituting the velocities in and integrating from x to x_E, the resulting equation is,

$$H^2 + \frac{\gamma_2}{\gamma_3} I^2 + \frac{\gamma_1}{\gamma_3} h_1^2 = H_0^2 + D_0^2(x, y) \tag{2.31a}$$

$$H^2\left[1 + \frac{\gamma_2}{\gamma_3}\frac{I^2}{H^2} + \frac{\gamma_1}{\gamma_3}\frac{h_1^2}{H^2}\right] = H_0^2 + D_0^2(x, y) \tag{2.31b}$$

$$H = \frac{\left[H_0^2 + D_0^2(x, y)\right]^{\frac{1}{2}}}{\left[1 + \frac{\gamma_2}{\gamma_3}\frac{I^2}{H^2} + \frac{\gamma_1}{\gamma_3}\frac{h_1^2}{H^2}\right]^{\frac{1}{2}}} \tag{2.31c}$$

We now need to find values for h_1, h_2 and h_3 in terms of H to solve the equation. The velocities for layer 2 are,

$$u_2 = -\frac{1}{f}\frac{\partial}{\partial y}\left[\gamma_3(h_1 + h_2 + h_3) + \gamma_2(h_1 + h_2)\right] \tag{2.32a}$$

$$v_2 = \frac{1}{f}\frac{\partial}{\partial x}\left[\gamma_3(h_1 + h_2 + h_3) + \gamma_2(h_1 + h_2)\right] \tag{2.32b}$$

By solving the conservation of potential vorticity equation for layer 2, we can use the Jacobian relationship which was used in region 2. The step has been skipped but results in $\frac{f}{h_2} = G_2(A)$, where $A = \gamma_3(h_1+h_2+h_3)+\gamma_2(h_1+h_2)$. On the boundary, $\frac{f}{h_2(y_1)} = G_2(A(y_1))$. The boundary between the second and third region ($y = y_1$) is continuous; we can set $h_1 = 0$ and equate the two equations ($A = A(y_1)$):

$$\gamma_3(h_1+h_2+h_3)+\gamma_2(h_1+h_2)=\gamma_3(h_2(y_1)+h_3(y_1))+\gamma_2 h_2(y_1) \tag{2.33a}$$
$$\gamma_3 H+\gamma_2(h_1+h_2)=\gamma_3 H(y_1)+\gamma_2 h_2(y_1) \tag{2.33b}$$
$$H+\frac{\gamma_2}{\gamma_3}(h_1+h_2)=\left[1+\frac{\gamma_2}{\gamma_3}\frac{h_2(y_1)}{H(y_1)}\right]H(y_1) \tag{2.33c}$$
$$H(y_1)=\frac{H+\frac{\gamma_2}{\gamma_3}(h_1+h_2)}{\left[1+\frac{\gamma_2}{\gamma_3}\frac{h_2(y_1)}{H(y_1)}\right]} \tag{2.33d}$$

The equation can be solved using $h_3(y_1)=\frac{f_1}{f_2}H(y_1)$ and, therefore, $h_2(y_1)=\left(1-\frac{f_1}{f_2}\right)H(y_1)$. We also note that $h_1+h_2=H-h_3$. Furthermore, $h_3=\frac{f}{f_2}H$ still holds past y_1 which can be derived in a similar way to (2.19). Therefore, the equation is,

$$H(y_1)=\frac{1+\frac{\gamma_2}{\gamma_3}\left(1-\frac{f}{f_2}\right)}{1+\frac{\gamma_2}{\gamma_3}\left(1-\frac{f_1}{f_2}\right)}H \tag{2.34}$$

To find h_2 we need to equate the Jacobian identity over the boundary as well,

$$\frac{f}{h_2}=\frac{f_1}{h_2(y_1)} \tag{2.35a}$$
$$h_2=\frac{f}{f_1}h_2(y_1) \tag{2.35b}$$
$$h_2=\frac{f}{f_1}\left(1-\frac{f_1}{f_2}\right)H(y_1) \tag{2.35c}$$
$$h_2=\frac{f}{f_1}\left(1-\frac{f_1}{f_2}\right)\frac{1+\gamma_2\gamma_3^{-1}\left(1-\frac{f}{f_2}\right)}{1+\gamma_2\gamma_3^{-1}\left(1-\frac{f_1}{f_2}\right)}H \tag{2.35d}$$

Trivially, $h_1=H-h_3-h_2$, thus we can substitute h_1, h_2 and h_3 back into (2.31c) to find H. For completeness, the analytical solution for H in the third region is,

$$H=\left[\frac{(H_0^2+D_0^2(x,y))}{F(y)}\right]^{\frac{1}{2}} \tag{2.36a}$$
$$F(y)=1+\frac{\gamma_2}{\gamma_3}\left(1-\frac{f}{f_2}\right)^2+\frac{\gamma_1}{\gamma_3}\left\{1-\frac{f}{f_2}-\frac{f}{f_1}\left(1-\frac{f_1}{f_2}\right)\left[\frac{1+\gamma_2\gamma_3^{-1}(1-f/f_2)}{1+\gamma_2\gamma_3^{-1}(1-f_1/f_2)}\right]\right\}^2 \tag{2.36b}$$

The Shadow zone:

The shadow zone for the third region has not been derived in detail due to its complexity. The general equation separating the ventilated area from the shadow zone can be found by setting $H=H_0$ and rewritten as,

$$D_0^2(\tilde{x}_3,y)=(F(y)-1)\,H_0^2 \tag{2.37}$$

The shadow zone is divided into two areas. In the area closest to the eastern boundary (R): layer 3 is stagnant, layer 2 conserves potential vorticity and layer 1 is forced by the wind. This results in the equations,

$$h_2 = \frac{f}{f_1}(h_1 + h_2) \tag{2.38a}$$

$$h_1 = (1 - \frac{f}{f_1})(h_1 + h_2) \tag{2.38b}$$

where the Sverdrup relation implies,

$$(h_1 + h_2) = (\gamma_3\gamma_2^{-1})^{\frac{1}{2}} \frac{D_0(x, y)}{\left[1 + \gamma_1\gamma_2^{-1}(1 - f/f_1)^2\right]^{\frac{1}{2}}} \tag{2.39}$$

The area M is between the ventilated area and R, where the eastern boundary is defined as,

$$D_0^2(\tilde{x}_2, y) = \frac{\gamma_2}{\gamma_3}\left(1 - \frac{f_1}{f_2}\right)^2 H_0^2 \left[1 + \frac{\gamma_1}{\gamma_2}\left(1 - \frac{f}{f_1}\right)^2\right] \tag{2.40}$$

This is the potential vorticity trajectory in layer 2 that comes from the intersection between $\tilde{x}_3(y)$ and the outcrop of layer 1. Within this region, the potential vorticity lines of layer 2 originate from the left of the intersection and, therefore, H is not constant. This changes the equation for h_2,

$$h_2 = \left(1 - \frac{f_1}{f_2}\right) H \tag{2.41}$$

Using the conservation of potential vorticity, this can be solved in a similar way to the solution in region 2. Therefore,

$$h_2 = \frac{f}{f_1}\left[H_0 + \frac{\gamma_2}{\gamma_3}(h_1 + h_2)\right] \frac{(1 - f_1/f_2)}{[1 + \gamma_2\gamma_3^{-1}(1 - f_1/f_2)]} \tag{2.42a}$$

$$h_1 = (h_1 + h_2)\left\{1 - \frac{f}{f_1}\frac{\gamma_2}{\gamma_3}\frac{(1 - f_1/f_2)}{[1 + \gamma_2\gamma_3^{-1}(1 - f_1/f_2)]}\right\} - H_0\frac{f}{f_1}\frac{(1 - f_1/f_2)}{[1 + \gamma_2\gamma_3^{-1}(1 - f_1/f_2)]} \tag{2.42b}$$

The Sverdrup equation can be solved creating a quadratic equation for $h_1 + h_2$,

$$h_1 + h_2 = \left\{\frac{\gamma_1}{\gamma_2}ab + \left[\frac{\gamma_3}{\gamma_2}D_0^2\left(1 + \frac{\gamma_1}{\gamma_2}a^2\right) - \frac{\gamma_1}{\gamma_2}b^2\right]^{\frac{1}{2}}\right\} \times \left(1 + \frac{\gamma_1}{\gamma_2}a^2\right)^{-1} \tag{2.43a}$$

$$a = 1 - \frac{f}{f_1}\frac{\gamma_2}{\gamma_3}\left[\frac{(1 - f_1/f_2)}{1 + \gamma_2\gamma_3^{-1}(1 - f_1/f_2)}\right] \tag{2.43b}$$

$$b = H_0\frac{f}{f_1}\left[\frac{(1 - f_1/f_2)}{1 + \gamma_2\gamma_3^{-1}(1 - f_1/f_2)}\right] \tag{2.43c}$$

2.6 Generalisation of regions

The process outlined above can be seen to be similar for regions 1, 2 and 3. The fourth regions was also found outside the shadow zone, which provided evidence that we understood the model sufficiently. An iterative solution was developed during the project for the ventilated areas. This aimed at solving the LPS model for an arbitrary number of layers. Unfortunately, there was not enough time to test the solution.

First, we define the notation: N_L is the number of layers, N is the maximum layer, R is the region number and L is the Lth layer. Note, the region number is labelled with the same number as the top layer; therefore, the region number decreases. H (the depth of the layer) and h (the height of the layer) can be written out formally using sums,

$$h_{L=R} = H_{N,R} - \sum_{l=0}^{N-L-1} h_{N-l,R} \tag{2.44a}$$

$$h_{L=N,R} = \frac{f}{f_{L-1}} H_{N,R} \tag{2.44b}$$

$$H_{L,R} = H_{N,R} - \sum_{l=0}^{N-L-1} h_{N-l,R} \tag{2.44c}$$

The solution for the height of the layer in the ventilated region is,

$$h_{L,R} = \frac{f}{f_R} \frac{h_{L,R+1}(y_{r=R})}{H_{N,R+1}(y_{r=R})} H(y_{R+1})_L \tag{2.45a}$$

$$H(y_R)_L = \frac{\sum_{l=0}^{N-L} \gamma_{N-l} \frac{H_{N-l,R}}{H_{N,R}}}{\sum_{l=0}^{N-L} \gamma_{N-l} \frac{H_{N-l,R}(y_{r=R})}{H_{N,R}(y_{r=R})}} H_{N,R} \tag{2.45b}$$

where,

$$\frac{H_{L,R}(y_r)}{H_{N,R}(y_r)} = 1 - \sum_{l=0}^{N-L-1} \frac{h_{N-l,R}(y_r)}{H_{N,R}(y_r)} \tag{2.46a}$$

$$\frac{h_{L,R}(y_r)}{H_{N,R}(y_r)} = \frac{h_{L,R}}{H_{N,R}}, \text{ where } f = f_r \tag{2.46b}$$

and the depth of layer N is,

$$H_{L=N,R} = \frac{[H_0^2 + D_0^2(x,y)]^{\frac{1}{2}}}{\left[\frac{1}{y_N} \sum_{l=0}^{N-N_L} \gamma_{N-l} \frac{H_{N-l,R}}{H_{N,R}}\right]^{\frac{1}{2}}} \tag{2.47}$$

The set of rules outlined above can be implemented as an iterative algorithm on a computer. A schematic showing how the generalisation can be applied to the cross-section is shown below.

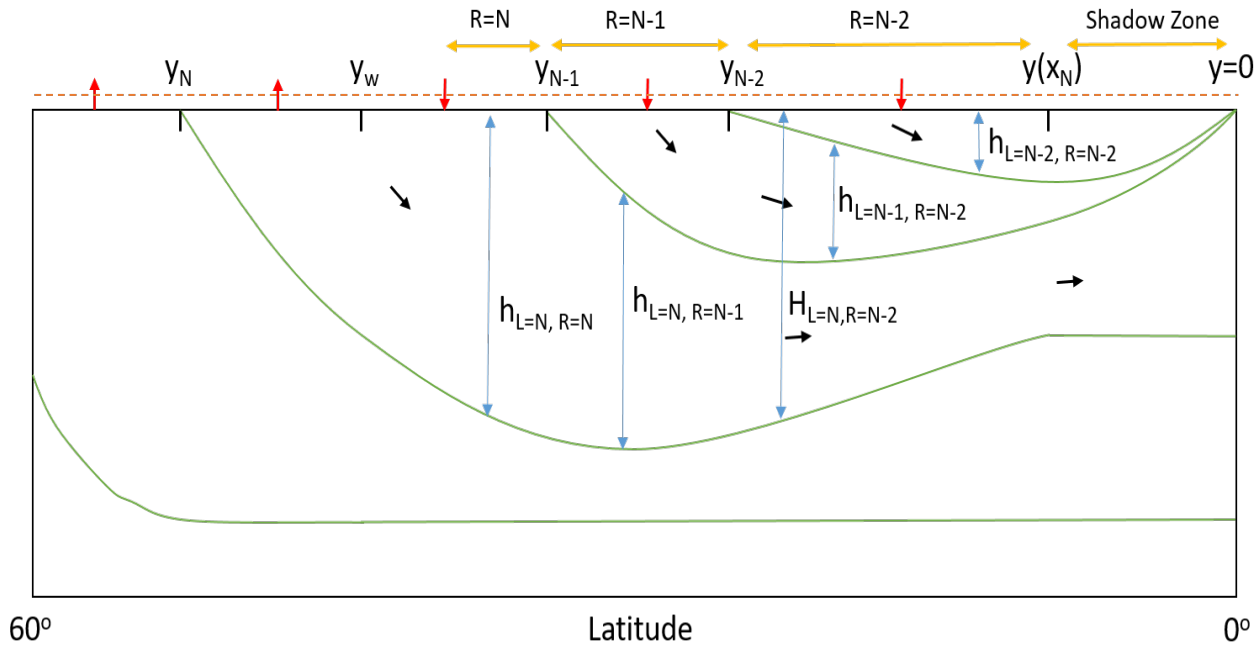

Figure 2.2: The cross-section to the LPS model at a constant latitude. The annotations show how the generalisation can be applied to solve for N layers.

Chapter 3

Method

3.1 Argo

This project relied on real data from ocean observations to compare to the theoretical model. The observational data used was from Argo, a project that aims to measure the temperature and salinity of the upper 2000m of the ocean. Currently, there are 3779 floats active, profiling the ocean. The deployment began in 2000 and is a major component of observing the ocean [12].

The temperature and salinity of each point in the ocean (latitude, longitude and depth) was averaged over time, for this project. As there is no time dependence within the LPS model, this allowed anomalous data to be negligible. The Argo data was transformed using a python package. The package, known as Gibbs-SeaWater (GSW) Oceanographic Toolbox, uses the temperature and salinity to find the density [13]. These densities were found for discrete coordinates and depths in the ocean. As the LPS model uses discrete density layers, the same layers were chosen for the Argo data using the densities. Therefore, a direct comparison between the depth, height and potential vorticity of each layer could be analysed visually and numerically.

3.2 The model

The LPS model was developed in python. The complexity of the model was gradually increased during the analysing process to understand which parts of the model made the most significant impacted on the solution. The North Atlantic Ocean was initially investigated. There were five concepts within the model which were explored: the number of layers, the eastern boundary, the Ekman pumping, the layer densities, and the outcrop regions. The complexity of these concepts were adjusted to see their impacts. Using the same technique the North Pacific Ocean was also investigated drawing on the most significant results. The potential vorticity of layer 3 was used for the majority of the results because this parameter held the most amount of information about the accuracy of the model.

3.3 Number of layers

The number of layers was a crucial parameter in this model. The model used discrete density layers which were immiscible and all frictional coupling between the layers was ignored. The number of layers was limited by the complexity of the derivations involved in finding an analytical solution to the shadow zone. The minimum number of layers that could be used was two, otherwise, there would be no shadow zone. As the number of layers tended to infinity, we would expect the solution to converge onto the continuous model. This has been derived by R. X. Huang, which parallelled the LPS and PY models [5]. Using the solutions for two and three layers, we were able to analyse the impact of increasing the number of layers.

In the theory section, we discuss the possibility of extrapolating the solution to create an algorithm for N discrete layers. Unfortunately, there was not enough time to test the algorithm and a solution for the shadow zone was not found. A further investigation would explore whether more layers improved the solution of the model compared to the Argo data and the continuous solution.

3.4 Eastern boundary

The model required an eastern boundary to find the solution. This boundary was used as the point to which the Ekman pumping was integrated. The physical representation of this line was the coastline of the North Atlantic Ocean which is the UK, France and Spain. Unfortunately, the eastern boundary has to be a straight line with fixed longitude for the solution to be valid. This was because the velocity of the fluid going into or out of the eastern boundary must be zero. If there was a sudden step in the coastline, this could lead to fluid movement into the boundary. Thus, a straight line with constant longitude must be used. Although, this boundary did not represent the coastline well. The impact of this was quantified and any atypical solutions that could be attributed to the approximation were presented in the results.

3.5 Ekman pumping

Ekman pumping is the downwards forcing on the water from the Ekman layer. This layer separates the highest layer, defined in the model, with the ocean's surface. Within the ocean, Ekman depths are 50m or less. The Ekman layer couples the atmosphere to the ocean via frictional forces exerted by the wind. These spatial variations in the wind cause spatial variation in the Ekman transport which results in an exchange of fluid with the ocean interior. This exchange is known as Ekman pumping. Therefore, from the Ekman's theory, the pumping generated from the Ekman layer forces the ocean interior circulation [9].

Originally, the Ekman pumping was assumed to be constant throughout the ocean. A more realistic estimate of quadratic pumping, in latitude, was implemented.. Finally, a modelled Ekman pumping was implemented. This model provided much more realistic values which could be used within the LPS model. Although, the disadvantage was that the resolution of the model had to be decreased significantly as it was now limited by the

resolution of the Ekman pumping. This sacrifice was compared to the improvement in the values for the pumping compared to the quadratic approximation. Furthermore, the modelled values allowed us to observe coupling between the atmosphere and the ocean's depth from the Ekman layer.

3.6 Layer densities

The original density layers chosen were straight from the LPS paper, using the three-layer model. Note, that the calculations for the γs were incorrect, in that paper, on Table 1. Initially, these layers were modelled and compared to the Argo data. The paper states that these layers were chosen arbitrarily; therefore, our proposal was to use new density layers found from Argo. Initially, the layers were adjusted until the model fitted that data. This provided a case that the layers can be fitted well from specifically chosen density layer; therefore, the LPS model can be used to model the ocean. Unfortunately, we required better reasoning for choosing the density layers other than fitting the data. Therefore, the boundary conditions were used as a basis for finding the new density layers. Using the Argo data, appropriate density layers were chosen from analysing the eastern boundary and y_3. The boundary conditions used to decide these layers were:

1. The bottom of layer 1,2 - zero depth on the eastern boundary.
2. The bottom of layer 3 - $H = H_0$ where $D_0 = 0$.
3. The bottom of layer 4 - constant depth, with no vertical movement.

If y_w (the line of $w_e = 0$) had a constant latitude, this enabled the y_w line to coincide with D_0. Therefore, the bottom of layer 3 should have a constant depth along y_w and the eastern boundary of H_0. The bottom of the third layer was taken as the pycnocline, the highest gradient of density with respect to depth. This boundary also separates layer 3, which is driven by the wind, and layer 4 which is stagnant. Therefore, correctly identifying it is critical to the success of the model. After changing the density layers, new γs, outcrop regions and H_0 were found.

3.7 Outcrop regions

The final parameter analysed was the outcrop regions. These define where the individual density layers start when moving southwards. Initially, the regions in the LPS paper were used but these had to change with different density layers. Our analysis was investigated south of y_w and, therefore, there were only two outcrop regions used: y_2 and y_1. Although, the location of y_3 was checked for consistency that it was north of y_w otherwise an incorrect layer 3 had been chosen. The theory behind the outcrops was from Stommel's demon. This suggests that the outcrop lines should be taken from the observations in late winter rather than the average position of the outcrop lines. The demon, which was the mixed layer, only allows a narrow range of densities to subduct at any geographical location [14]. By only averaging the Argo data for winter, the outcrops according to Stommel's demon were found.

The outcrops were found to be slanted in the North Atlantic Ocean. An investigation was performed to measure the effect on the potential vorticity of an outcrop that did not have a constant latitude $y_2(x)$. This provided us with a challenge mathematically and computationally because H could no longer be solved analytically; this is shown in the appendix. A new line was created for $y_2(x)$ which slanted from 45° to 35° latitude across the North Atlantic Ocean. Along this line, the potential vorticity and H (the depth of layer 3) were found. A graph was plotted of the potential vorticity against H at each point along the line.

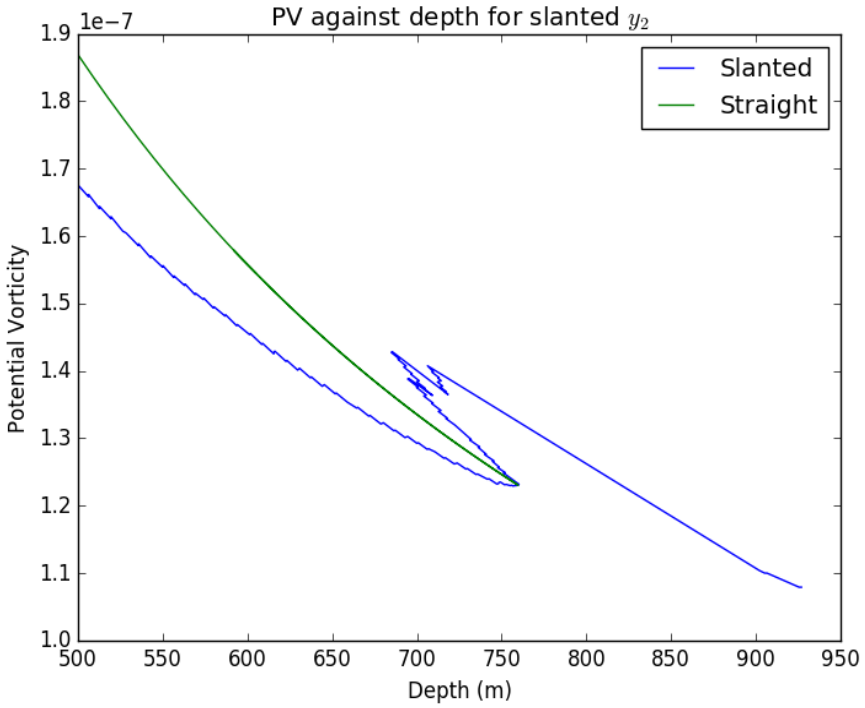

Figure 3.1: The potential vorticity (SI units of $m^2s^{-1}Kkg^{-1}$) against the depth for the straight and slanted y_2. The new density layers were used for the North Atlantic Ocean. The straight y_2 was at 40° latitude and the slanted was between 45° to 35°. The curved shape was a known phenomenon and was mentioned in the LPS paper. A best-fit line was plotted through it to the best of its ability; although, this will have caused uncertainties in the values of the function.

Figure 3.1 represents the function $G_3(H)$ in (2.19) which was previous found to be $\frac{f(y_2)}{H(y_2)}$ along a constant latitude (straight). $G_3(H)$ showed that the potential vorticity of $y_2(x)$ folded back to intersect a fluid trajectory more than once. This was a known phenomenon that was mentioned in the LPS paper with no solution. Therefore, the data points were reordered to, somewhat, remove this effect and a polyfit line was fitted through the new line. The new line was equivalent to an average of the line found. An optimisation had to be performed on the value of H for each point in the ocean to find the solution. This significantly increased the run time which comprised the resolution of the model further. Fortunately, sufficient data was gathered to investigate whether the slanted outcrop would improve the prediction of the LPS model.

Chapter 4

Results

4.1 The model

The solution to the LPS model was plotted to represent Figure 2.1. A quadratic approximation was used for the Ekman pumping. This allowed a clear comparison due to the high resolution. Furthermore, a similar image was created using Argo. Density layers have been chosen from the LPS paper.

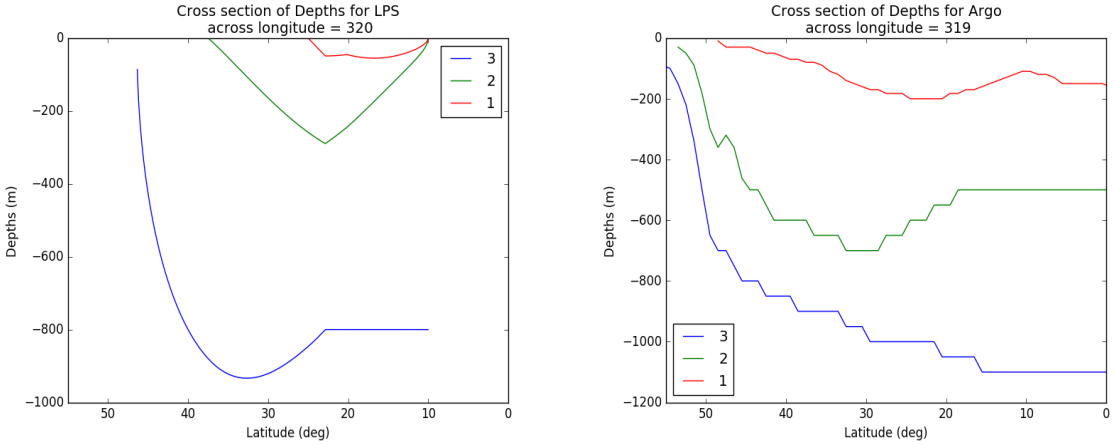

(a) LPS with quadratic Ekman pumping

(b) Argo cross-section

Figure 4.1: The graphs are from the cross-section of the LPS model and the Argo data through the center of the North Atlantic Ocean. The layers do not conform well. Layer 3 from the LPS seems more similar to layer 2 from the Argo.

The cross-section from the LPS model showed how each density layer enters. The quadratic Ekman pumping was zero at y_w (40°). The Ekman pumping increased towards (25°) with a value of 30 m/year and decreased to zero at 10° latitude. This shape created a maximum depth in the cross-section around 33° for layer 3. The shadow zones were seen via the sudden changes in the depth of the layers; these layers were still continuous over these areas. In the shadow zone, layer 3 increased past H_0 which caused $H = H_0$ as stated in the theory. Therefore, the depth of layer 3 did not vanish with zero Ekman pumping.

The same density layers used on the Argo data did not produce the same picture. Layer 3 kept decreasing until it became flat at the shadow zone. Layer 2 appeared to be like layer 3, with a minimum around 30° latitude; the constant value coincided with the

approximate value of zero Ekman pumping at 40°. Layer 1 did not increase to the surface like the LPS model predicted. All the layers outcropped much further south than was estimated. This could be due to the data being averaged overall time instead of just the winter using Stommel's demon. The quadratic assumption used might not have been the correct shape or be the right size. Initially, there was not a vast similarity between the model and the data.

Towards the low latitudes, the model did not predict the ocean well because the geostrophic assumption was not valid. This required that the inertial forces were less than the Coriolis force. At low latitudes, the inertial forces were much greater in the ocean caused by the sea having a higher velocity. This led to a Rossby number greater than one, where the geostrophic assumption was invalid. Therefore, we limited ourselves to analysing latitudes greater than 10°.

4.2 Number of layers

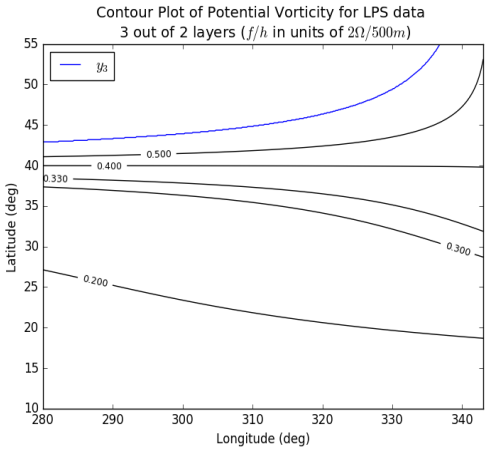

(a) One layer solution of layer 3

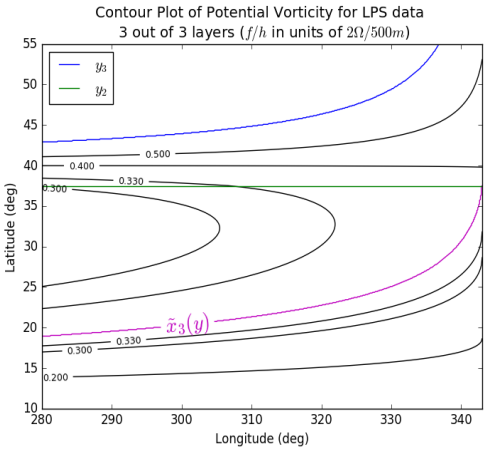

(b) Two layer solution of layer 3

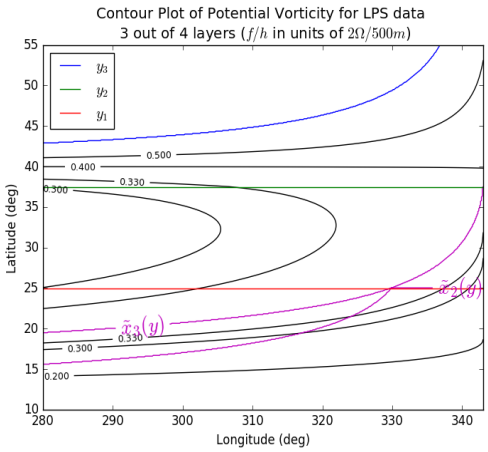

(c) Three layer solution of layer 3

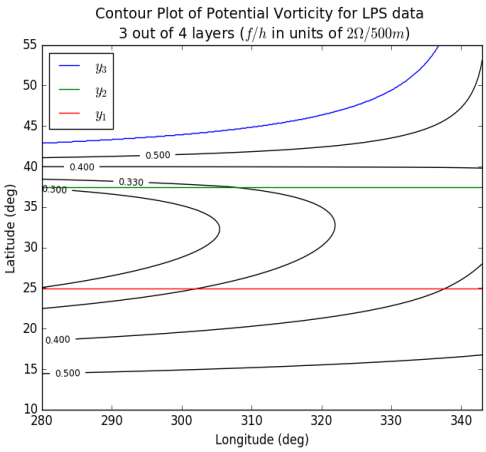

(d) Three layer solution of layer 3 with No Shadow Zone

Figure 4.2: This figure shows how increasing the number of layers changes the potential vorticity. The shadow zones can be seen in magenta. A comparison can be made with LPS solution without a shadow zone in (d) where the potential vorticity increases with the depth.

Increasing the number of layers from one to two dramatically changed the potential vorticity of the density layer. Layer 2 shielded layer 3 from the Ekman pumping; therefore, layer 3 conserved potential vorticity when it subducted and its potential vorticity changed direction. Thus, the layer was no longer being driven by the wind. The conserved potential vorticity contours curved from the top right corner of the y_2 outcrop to the bottom left because the conserved contours approximately followed constant height contours in layer 3. This was the shape of the height because of the quadratic Ekman pumping. Furthermore, the emergent shadow zone caused the bottom of the layer to be constant in this region; therefore, the potential vorticity decreased towards the equator instead of increasing. This was due to the Coriolis parameter decreasing to zero at the equator. This can be seen by comparing Figure (c) with Figure (d). The difference between the two and three layer solution was due to the change in the location of the shadow zone. The three-layer solution did not provide a vast difference in the shape compared to the two-layer solution. Nevertheless, it provided an extra dimension from which to make comparisons against the Argo data. Noting that the solution did not change significantly, it can be thought that an N-layered model will only change incrementally from the two-layer solution. This was a supposition; a further study could be performed to test if this is true.

The shape of the potential vorticity in the model for the three-layer solution coincided with the result from the Argo data found in Figure 4.5 (b). The potential vorticity contours moved south-west from the eastern boundary and the potential vorticity decreased towards the equator. This provided evidence that a shadow region was required. Layer 3 from Argo was still different from the model. This can be seen by the minimum in the model and the maximum in the Argo data. This could have been due to the values, chosen for the densities of layer 3, being incorrect. We must note that the solution of the LPS model was only valid if the potential vorticity contours originate from the outcrop of y_2. Therefore, the area west of the potential vorticity contour equal to 0.3 was not possible to model. This is shown by $x_s(y)$ in Figure 2.1 (b).

4.3 Eastern boundary

The straight, vertical eastern boundary did not represent the coastline well in the Atlantic. This was a fundamental limitation of the model which resulted in an underestimate of the depth. This was because the eastern boundary was taken further south than the coastline. An example of this will be seen later in the analysis where the shape of the contour lines did not match the Argo data. This phenomenon was particularly present in the southern region.

4.4 Ekman pumping

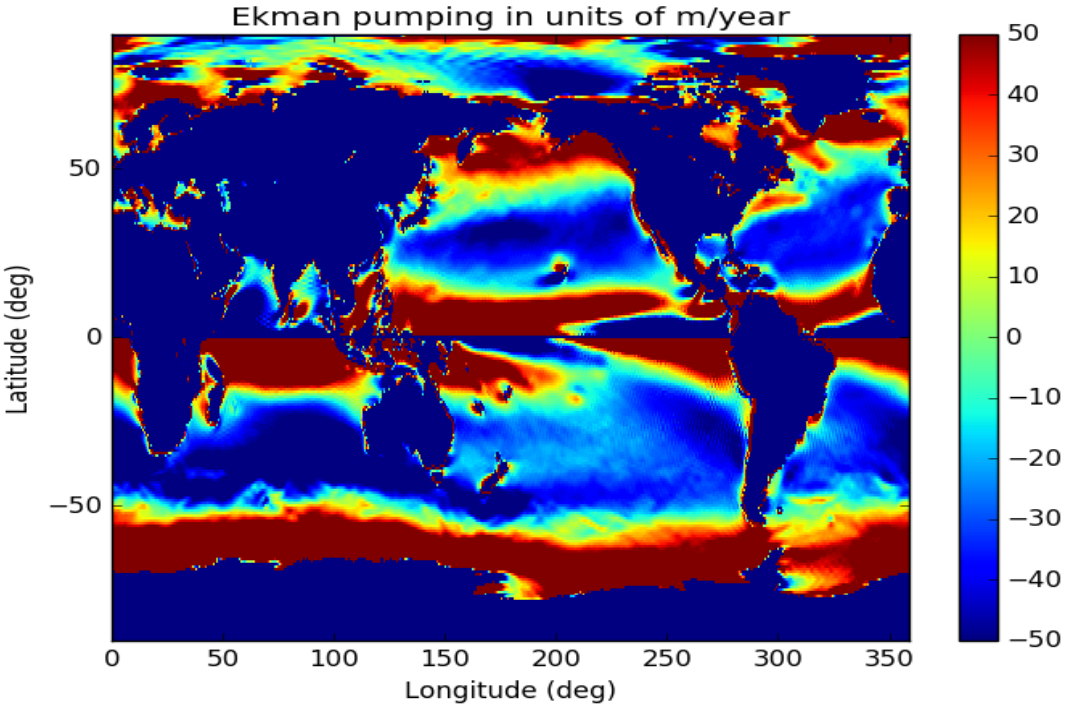

Figure 4.3: The modelled Ekman pumping which was used for w_e and was integrated to find D_0^2. This model is thought to be a very good representation of the actual Ekman pumping in throughout the ocean.

The Ekman pumping had upwards forcing in the higher latitudes and around the equator. This led to the depth of the density layers being forced upwards. Conversely, in the middle of this region, the pumping was downwards forcing which caused the depth of the layer to increase. Therefore, the density layers were expected to be deeper around 25°. This found in the LPS model and the Argo data. The change in direction of Ekman pumping was due to change in the winds. The northeasterly trade winds (blowing westwards), creating a downwards Ekman pumping in the mid latitudes whereas the westerlies create upwards Ekman pumping in the high latitudes [16]. The boundary between the pumping areas created a line of zero Ekman pumping (y_w). This line, shown in Figure 4.3, was diagonal within the North Atlantic. Unfortunately, this can not be modelled and, therefore, a limitation of the LPS model.

The modelled Ekman pumping can be seen to be approximately quadratic in shape from 0° to 55° latitude. This showed that a quadratic approximation was a valid assumption in preliminary tests. It represented the modelled Ekman pumping well compared to a constant value. The modelled data was used to find coupling between the atmosphere and the ocean. By comparing the LPS solution, using the actual Ekman values, with the Argo data, similarities that arose from the change of Ekman pumping were a result of coupling. This can be seen in the following sections.

4.5 Layer densities

The new density layers were found by analysing the Argo data. The eastern boundary was inspected to find density layers which abided by the strict boundary conditions inflicted from the LPS model.

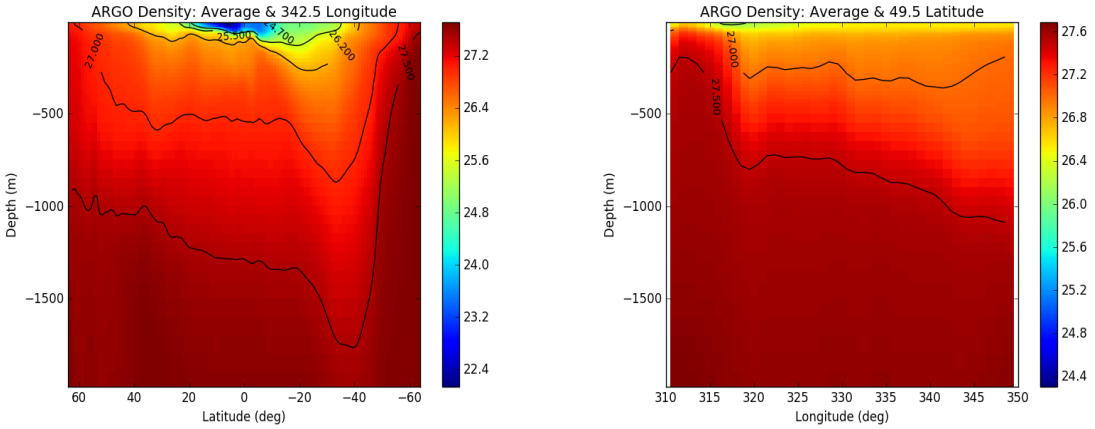

(a) Argo cross-section along the Eastern boundary (b) Argo cross-section along y_w

Figure 4.4: The Argo density layers can be seen on the eastern boundary and on y_2. These graphs can be used to find appropriate density layers for the LPS model. The densities are given in units of kgm^{-3} with respect to the density at 0 dbar.

The cross sections of the density, from the Argo data, showed that there was no perfect density layer that could be chosen for layer 3. Layer 3 needed to be constant along $D_0 = 0$; in this case, that was the eastern boundary and y_w shown in the diagrams. The best layer had a density of $1027kgm^{-3}$. The average value of the lines seemed to coincide more than any other density. Layers 1 and 2 were chosen from two different densities that originated from the surface on the eastern boundary. In Figure 4.5 (a), the densities have almost zero height on this boundary. Finally, layer 4 was found by looking for a layer that was relatively constant throughout the ocean. Figure 4.1 (b) showed that a density large enough would not be affected by positive Ekman pumping; therefore, this layer was stagnant in the ocean.

Table 4.1: Density parameters of the three-layer model in kg/m^3

Layer	North Atlantic	North Pacifc
1	1024.7 - 1025.5	1024.5 - 1025.2
2	1025.5 - 1026.2	1025.2 - 1025.7
3	1026.2 - 1027.0	1025.7 - 1027.0
4	1027.0 - 1027.5	1027.0 - 1027.4

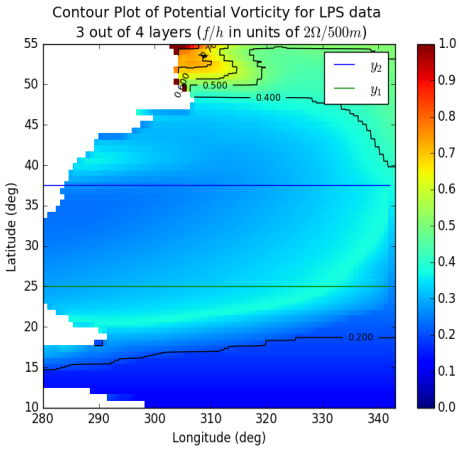

(a) PV for LPS using Old Density Layers

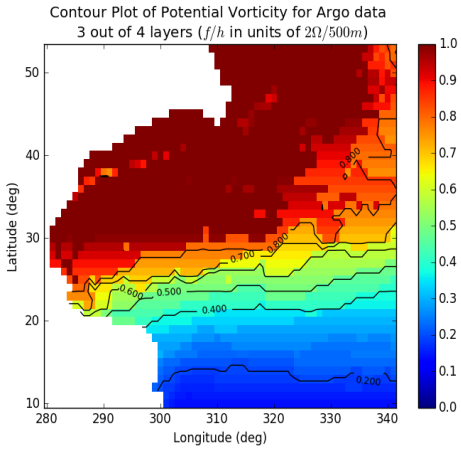

(b) PV for Argo using Old Density Layers

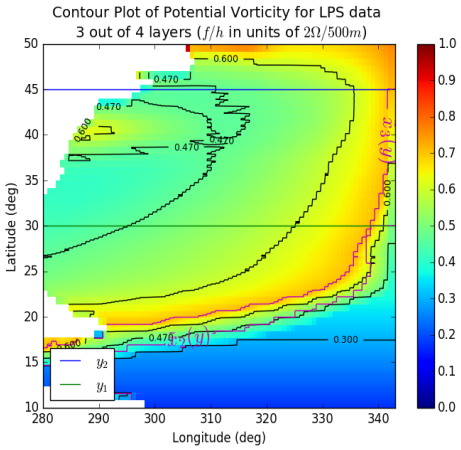

(c) PV for LPS using New Density Layers

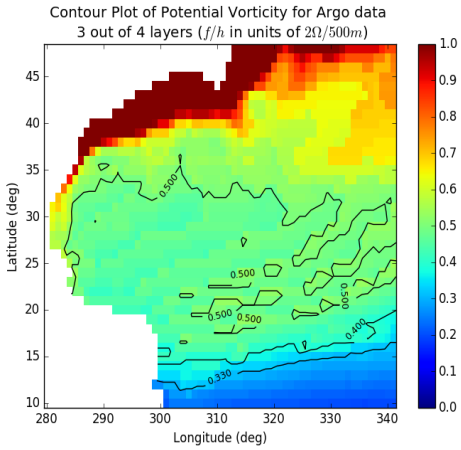

(d) PV for Argo using New Density Layers

Figure 4.5: These diagrams show the comparison between the LPS and Argo data before and after the change of density layers. The latter figures show a much better match than the previous ones.

These density layers made a vast improvement to the solution for layer 3 compared to the Argo data. Previously, layer 3 was using density layers which were similar to layer 4 values. Therefore, layer 3 was far too static, thus not deepening far enough which created an incorrect solution for the potential vorticity. The shadow zone can be seen very clearly with the potential vorticity contours decreasing southwards and sweeping across in a south-westerly direction. This would not be possible with a one layer model. Layer 1, 2 and 4 also changed and better matched the depth and potential vorticity compared to the Argo data. Furthermore, the scatter comparison shown further on in the results clearly emphasises the difference. As previously mentioned, the area enclosed by the potential vorticity contour equal to 0.47, where the conserved potential vorticity lines originate south of the outcrop, can not be modelled. Therefore, the minimum found in the LPS model would not be found in the Argo data.

Unfortunately, these layers were still not perfect. The size of the North Atlantic Ocean, the location of y_w and the shape of the eastern boundary did not allow for a sufficiently large enough area to find perfectly conforming density layers. Fortunately, the North Pacific Ocean was large enough to provide better density layers which were also analysed.

4.6 Outcrop regions

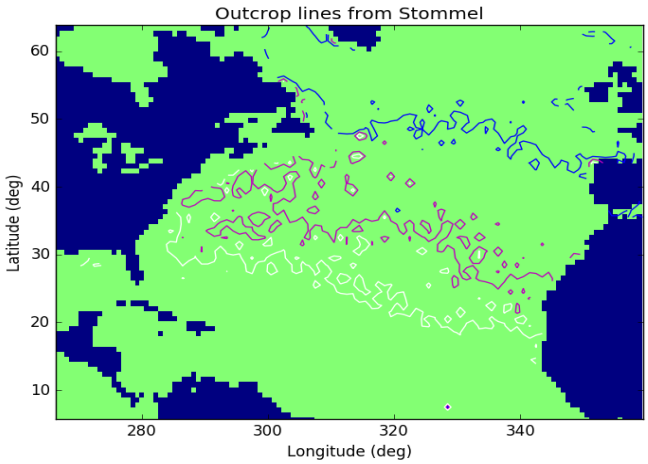

Figure 4.6: This graph contains the outcrops calculated from Stommel's demon. A value for the outcrops were taken using these lines.

The outcrops found using Stommel's approximation can be seen in the diagram. These lines showed the approximate value of the outcrop which should be chosen by averaging the winter densities. The outcrops were found to be diagonal; therefore, the northernmost latitude was taken as the value for the outcrop line. The outcrop for y_3 showed that the value chosen was appropriate because it outcropped north of y_w and, therefore, had a non-zero depth at y_w. The value of the outcrop was just north of y_w, therefore it still was not a perfect density layer. The outcrop of y_2 was 45° latitude and y_1 was 30°.

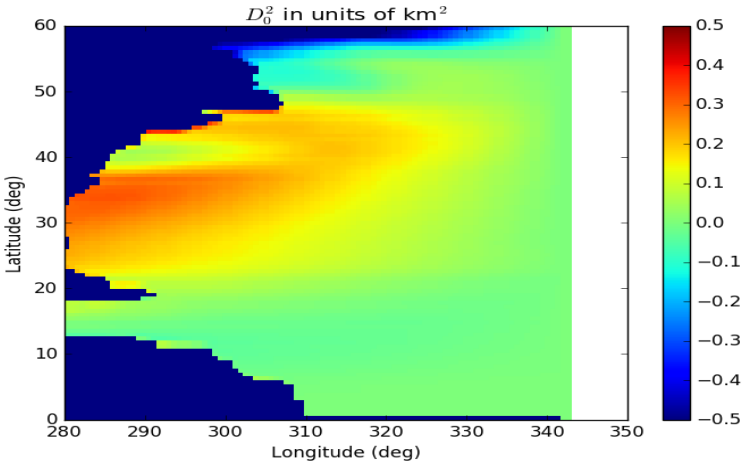

Figure 4.7: This graph shows the value of D_0^2 through the North Atlantic Ocean.

The value of D_0^2 was calculated across the North Atlantic Ocean. The boundary between positive and negative D_0^2 was were the depth of layer 3 was constant. This was approximately a straight line and agreed with the zero Ekman pumping line. This can be used to assume that H was constant along y_w.

A further investigation was performed to see whether a slanted y_2 outcrop would affect the solution significantly.

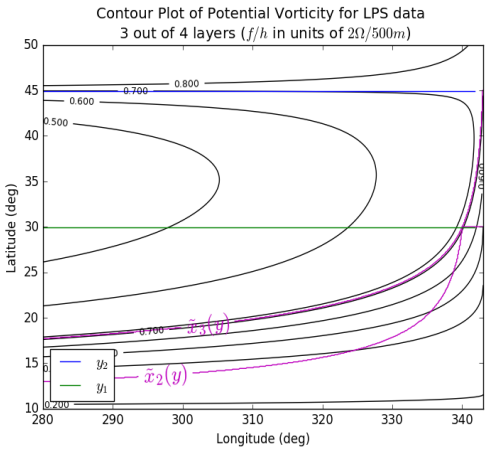

(a) Straight y_2 with quadratic Ekman pumping

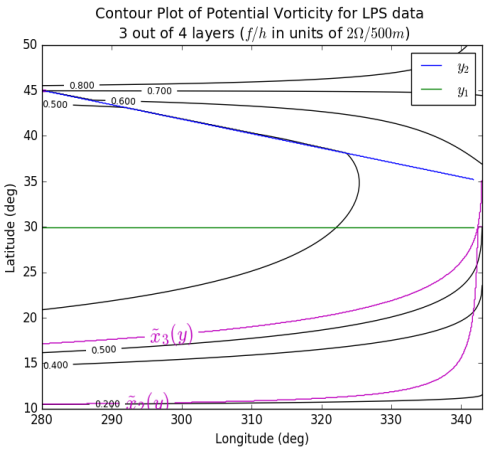

(b) Slanted y_2 with quadratic Ekman pumping

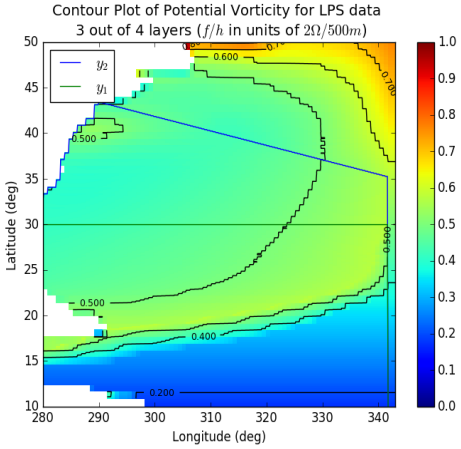

(c) Slanted y_2 with real Ekman pumping

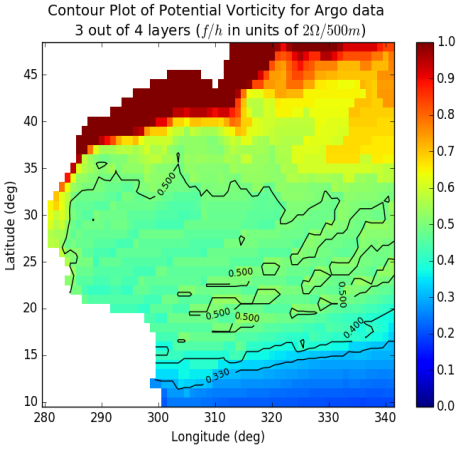

(d) Argo PV for layer 3

Figure 4.8: The diagram shows how a slanted y_2 changes the potential vorticity contours in the model. The slanted y_2 models the Argo data better than a straight line.

Graphs (a) and (b) were similar which showed that the slanted outcrop did not change the solution vastly. The potential vorticity contours were more curved in the north-east corner. This change coincided better with the potential vorticity contours found in the Argo data and, therefore, there was evidence to believe that this improved the model. The inner most contours can be seen to enter further east compared to the straight line. This was due to a high potential vorticity following the outcrop down, further into the Atlantic ocean. In the latter half of the graph, the shadow zones were slightly different with a larger area for zone M. This was because the zone originated from an outcrop further south on the eastern boundary. Unfortunately, the solution comprised the resolution of the data so further analysis was not performed. A longer time frame would be required to run the model to a sufficient resolution.

4.7 Pacific

The North Pacific Ocean was analysed because the size and shape of the ocean was much larger than the North Atlantic Ocean. This allowed for a greater area to compare with the observed data. The eastern boundary and the coastline coincided much more closely. This enabled the density layer to be found and, therefore, a much closer comparison to be made. The cross-section of the density layers and the outcrops is shown in the appendix with the final values in Table 4.1.

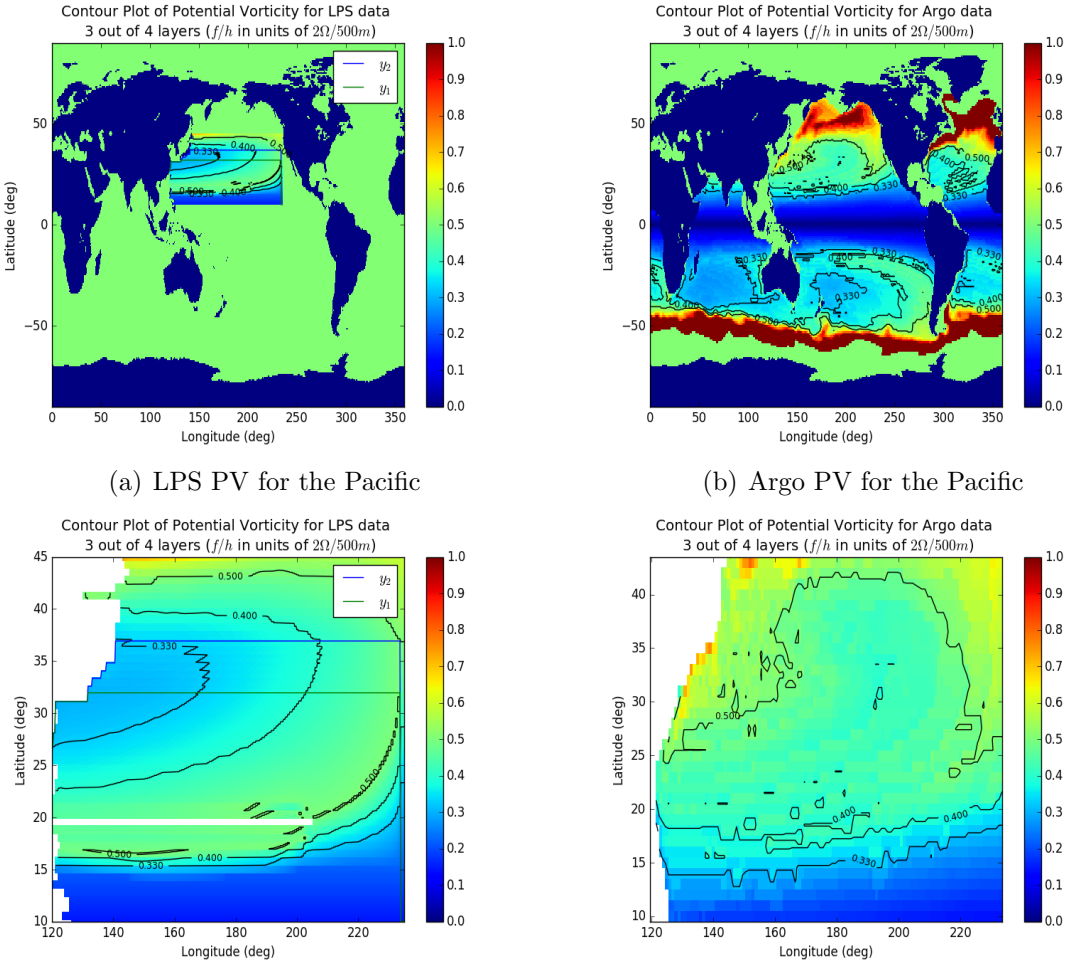

(a) LPS PV for the Pacific

(b) Argo PV for the Pacific

(c) LPS PV for the Pacific zoomed

(d) Argo PV for the Pacific zoomed

Figure 4.9: The diagrams show the potential vorticity of the third layer in the North Pacific Ocean. The LPS models the observed Argo data well for the areas which are valid.

This presented a very close comparison to the major parts of the ocean. Again, the potential vorticity lines swept west and decreased towards the south providing evidence of a shadow zone in the Argo data. An issue with the real Ekman values arose in the North Pacific Ocean. This occurred around Hawaii where the values were positive, implying that the sea was being forced upwards. When these values were integrated across the ocean, a line of much higher values was found which did not correspond to results seen in Argo. This could be anomalous because there was no other case of this occurring, or an inconsistency in the model. There were similarities in the potential vorticity lines around Hawaii which could be due to coupling between the atmosphere and ocean. At 20°

latitude on the eastern boundary, the potential vorticity lines of the LPS protrude further west than in the Argo. This could be a result of the eastern boundary not following the coastline and, therefore, causing the depth of layer 3 to be too shallow.

The most significant result was the difference between the two graphs. The area that could not be predicted by the model and anomalous values in the observed data coincided almost perfectly. This area was west of the potential vorticity contour equal to 0.33 where there was a minimum in the LPS and a maximum in the Argo. This area would require a different model which used the western boundary. To our knowledge, there has not been a model which can predict this. A further investigation could find a solution to this area.

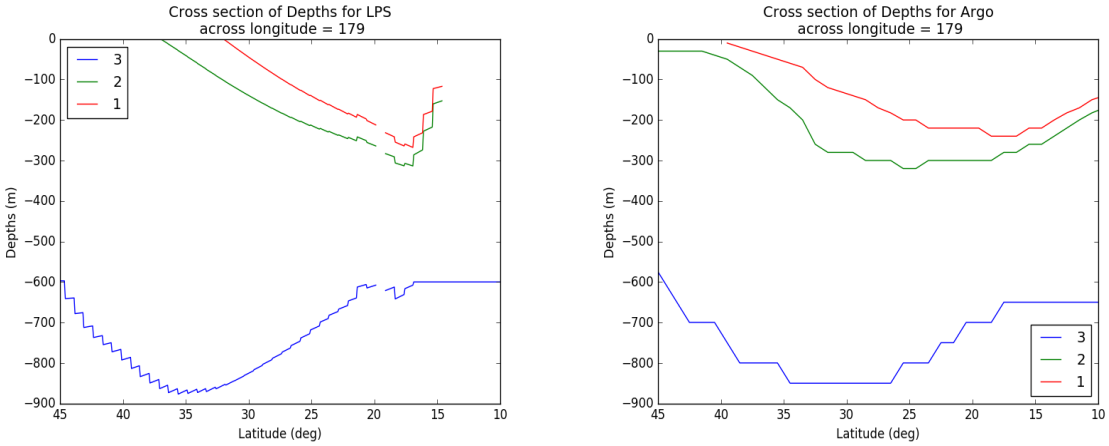

(a) LPS Pacific with actual Ekman pumping

(b) Argo cross-section

Figure 4.10: These are cross-sections through the center of the North Pacific Ocean. The modelled values conform well to the Argo data.

The cross-sections of the layers through the North Pacific Ocean were very similar. The bottom of layer 3 was constant after $\tilde{x}_3(y)$ as predicted by the shadow zone. This was a considerable improvement from Figure 4.1. The prediction for the lower latitude diverged from the Argo data. This could be due to the geostrophic approximation not being valid below 17° latitude.

4.8 Analytical comparison

The analytical comparison was performed to compare all four layers with the observed data. This allowed a clear comparison to be made whether the LPS modelled the North Atlantic and the North Pacific Ocean well. Two parameters could be compared: the height and the depth. The potential vorticity ($\frac{f}{h}$) could not be compared due to the large range of values in the height.

Figure 4.11 showed the significant improvement in the depths and heights from the original LPS paper. The main difference was changing the density layers to conform to the boundary conditions. In Figure 4.11 (f), the values under the line in layer 3 were a result of an overestimate in the heights from the model. The overestimate could have been attributed to the region that was supposed to be excluded from the analysis, as mentioned above. A further study could remove this area, therefore providing evidence that the LPS

solution models the Pacific ocean well within its constraints. Statistical analysis on the graphs has been left for a further investigation.

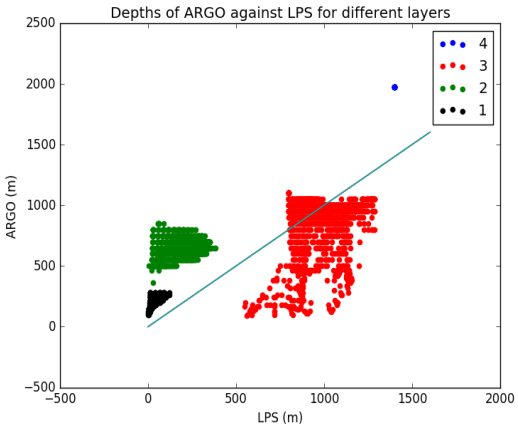

(a) Atlantic Depths with Densities from Paper

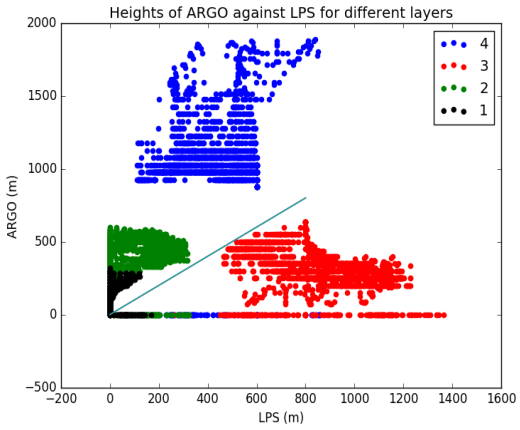

(b) Atlantic Heights with Densities from Paper

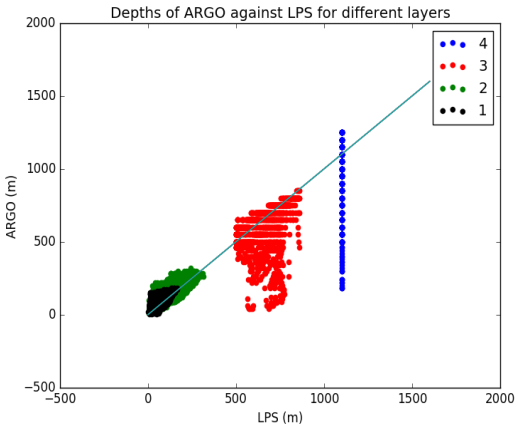

(c) Atlantic Depths with New Densities

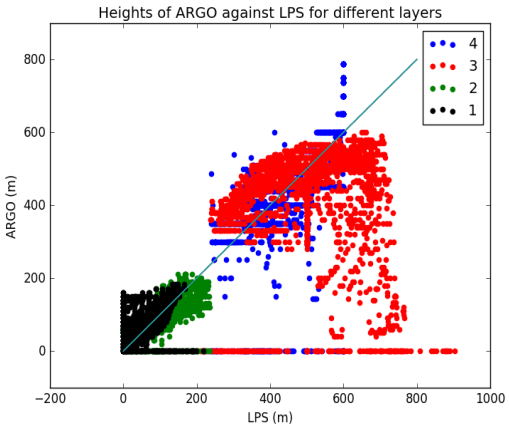

(d) Atlantic Heights with New Densities

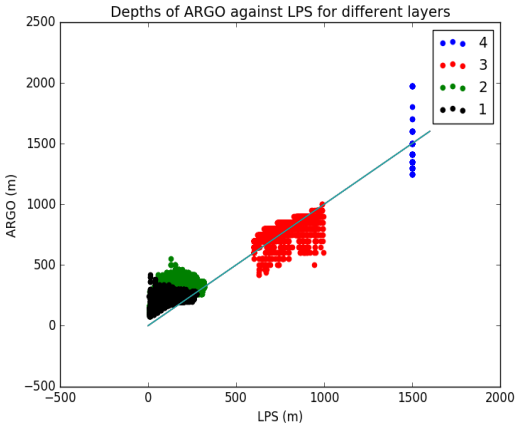

(e) Pacific Depths with New Densities

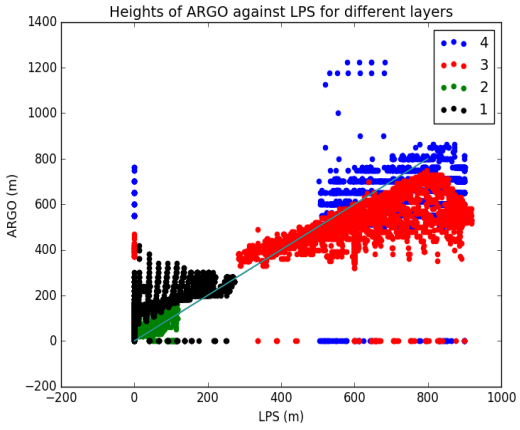

(f) Pacific Heights with New Densities

Figure 4.11: The different scatter plots show how the layers changed with different densities. The line $y = x$ has been plotted. For a perfect match, the LPS and Argo values for each coordinate in the ocean would lie upon this line. Therefore, the closer the points were to this line, the better the model predicted the ocean. Initially, there was not a good comparison between the LPS model and the Argo data. The last two plots of the North Pacific Ocean show good similarity between the model and Argo data.

Chapter 5

Conclusion

This project aimed at investigating whether the LPS model could be used to predict the depth and height of discrete density layers throughout the ocean. The LPS model was compared to observational data from the Argo project which recorded the temperature and salinity across the ocean at different depths. The complexity was increased throughout this project by changing various parameters. These included: the number of layers, the eastern boundary, the Ekman pumping, the layer densities, and the outcrop regions. The most significant impact on the result was from the layer densities.

The LPS model provided an explanation for the decreasing potential vorticity towards the equator shown in the Argo data which can be seen in Figure 4.5 (d). This was due to the presence of the shadow zone which was a result of the boundary conditions of the model shown in Figure 4.2 (c). The shadow zone has previously been confirmed by looking at the oxygen levels in the ocean; in the shadow zone, the oxygen levels were much lower due to the region being unventilated. The North Atlantic was first analysed using the density layers from the paper. These layers were chosen arbitrarily therefore new layers were chosen due to the boundary conditions of the model. Perfect density layers could not be found from the Argo data in Figure 4.5. The model was, therefore, assumed to not work very well for this region but the change of density layers still made a significant improvement to the solution. The outcrops used within the model were found from Stommel's demon in Figure 4.6. This showed that a slanted y_2 outcrop was a better approximation for the North Atlantic. This was modelled and provided a slight improvement to the solution shown in Figure 4.8. The model was then used to analyse the North Pacific Ocean. The solution was found to model the Argo data well when given layers which conformed to the boundary conditions of the model. This can be seen in Figure 4.9. Furthermore, the model predicted an area in its solution that can not be solved. This area was very similar to an area in the North Pacific Ocean which produced the opposite result to that which one might expect. Scatter plots of the depth and height for all the layers were produced. This clearly showed the improvement made from changing density layers and provides evidence that the LPS model is the correct model to predict how density changes with depth over the ocean.

Further Investigation:

A number of questions were asked throughout the report which could be used for further investigation. Unfortunately, the timescale of this project did not allow the answers to be found. The questions included:

1. What is the effect of having many more layers?
2. Does a slanted y_2 significantly improve the model?
3. Without the area that can not be modelled, how does the statistical result improve?
4. Can you model this area using the western boundary?
5. Can you make a time dependent LPS model?

Acknowledgments

The author wishes to thank Arnaud Czaja for his generous support, supervision and guidance throughout the project, as well as, the observational data he provided for some of the findings.

Bibliography

[1] R. X. Huang, B. Qiu: *The Structure of the Wind-Driven Circulation in the Subtropical South Pacific Ocean* American Meteorological Society, 1998

[2] P. B. Rhines, W. R. Young: *Homogenization of potential vorticity*, J. Fluid Mech. (1982), vol. 122, pp. 347-367

[3] J. R. Luyten, J. Pedlosky, H.Stommel: *The Ventilated Thermocline*, Journal of Physical Oceanography, Volume 13, 1983

[4] J. Pedlosky, W. R. Young: *Ventilation, Poential-Vorticity Homogenization and the Structure of the Ocean Circulation*, Journal of Physical Oceanography, Volume 13, 1983

[5] R. X. Huang: *On Boundary Value Problems of the Ideal-Fluid Thermocline*, American Meteorological Society, 1988

[6] Lynne D. Talley: *Ventilation of the Subtropical North Pacific: The Shallow Salinity Minimum*, Journal of Physical Oceanography, Volume 15, 1985

[7] A. Gnanadesikan, J. L. Russell, F. Zeng: *How does ocean ventilation change under global warming?*, Ocean Sci., 3, 4353, 2007

[8] I. Mueller-Wodarg: *Fluid Dynamics*, Imperial College London, 2017

[9] J. H. Steele, S. A. Thorpe, K. K. Turekian: *Ocean Currents: A Derivative of the Encyclopedia of Ocean Sciences*, Academic Press, 2010

[10] B. J. Hoskins: *Towards a PV-θ view of the general circulation*, Tellus, 1991

[11] Ramana: *Applied Mathematics*, Tata McGraw-Hill Education, 2007

[12] Argo: *http://www.argo.ucsd.edu/*, [last visited: 26th April 2017]

[13] Thermodynamic Equation of Seawater - 2010: *http://www.teos-10.org/software.htm*, [last visited: 26th April 2017]

[14] J. Pedlosky: *Ocean Circulation Theory*, Springer Science & Business Media, 2013

[15] G. K. Vallis: *Atmospheric and Oceanic Fluid Dynamics*, Cambridge University Press, 2006

[16] George L. Pickard, W. J. Emery: *Descriptive Physical Oceanography*, Pergamon Press, 1990, pp. 161

Appendix

5.1 Sverdrup vorticity equation - step by step

Differentiating (2.3a),

$$\rho_n f u_n = -\frac{\partial P}{\partial y} \tag{5.1a}$$

$$\frac{\partial}{\partial x}\left(\rho_n f u_n\right) = -\frac{\partial^2 P}{\partial y \partial x} \tag{5.1b}$$

$$\rho_n f \frac{\partial u_n}{\partial x} = -\frac{\partial^2 P}{\partial y \partial x} \tag{5.1c}$$

Differentiating (2.3b),

$$\rho_n f v_n = \frac{\partial P}{\partial x} \tag{5.2a}$$

$$\frac{\partial}{\partial y}\left(\rho_n f v_n\right) = \frac{\partial^2 P}{\partial x \partial y} \tag{5.2b}$$

$$\rho_n \frac{\partial f}{\partial y} v_n + \rho_n f \frac{\partial v_n}{\partial y} = \frac{\partial^2 P}{\partial x \partial y} \tag{5.2c}$$

$$\rho_n \beta v_n + \rho_n f \frac{\partial v_n}{\partial y} = \frac{\partial^2 P}{\partial x \partial y} \tag{5.2d}$$

Combining (5.1) and (5.2),

$$\rho_n f \frac{\partial u_n}{\partial x} + \rho_n \beta v_n + \rho_n f \frac{\partial v_n}{\partial y} = -\frac{\partial^2 P}{\partial y \partial x} + \frac{\partial^2 P}{\partial x \partial y} \tag{5.3a}$$

$$f \frac{\partial u_n}{\partial x} + \beta v_n + f \frac{\partial v_n}{\partial y} = 0 \tag{5.3b}$$

$$\beta v_n = -f\left(\frac{\partial u_n}{\partial x} + \frac{\partial v_n}{\partial y}\right) \tag{5.3c}$$

$$\beta v_n = f \frac{\partial w_n}{\partial z} \tag{5.3d}$$

5.2 Velocities - Region 1

Using the hydrostatic equation,

$$\frac{\partial P_3}{\partial z} = -\rho_3 g \tag{5.4a}$$
$$\int_{z_A}^{0} \frac{\partial P_3}{\partial z} dz = -\int_{z_A}^{0} \rho_3 g dz \tag{5.4b}$$
$$P(0) - P_3 = -\rho_3 g (0 - z_A) \tag{5.4c}$$
$$P(0) - P_3 = -\rho_3 g z_A \tag{5.4d}$$

$$\int_{z_B}^{0} \frac{\partial P_3}{\partial z} dz = -\int_{z_B}^{0} \rho_3 g dz \tag{5.5a}$$
$$P(0) - P_4 = -\left(\int_{-h_3}^{0} \rho_3 g dz + \int_{z_B}^{-h_3} \rho_3 g dz \right) \tag{5.5b}$$
$$P(0) - P_4 = -\left(\rho_3 g h_3 - \rho_4 g h_3 - \rho_4 g z_B \right) \tag{5.5c}$$
$$P(0) - P_4 = g\left(\rho_4 - \rho_3\right) h_3 + \rho_4 g z_B \tag{5.5d}$$

Combing (5.4) and (5.5),

$$(P(0) - P_4) - (P(0) - P_3) = g\left(\rho_4 - \rho_3\right) h_3 + \rho_4 g z_B + \rho_3 g z_A \tag{5.6a}$$
$$P_3 - P_4 = g\left(\rho_4 - \rho_3\right) h_3 + \rho_4 g z_B + \rho_3 g z_A \tag{5.6b}$$
$$\frac{\partial P_3}{\partial x} - \frac{\partial P_4}{\partial x} = g\left(\rho_4 - \rho_3\right) \frac{\partial h_3}{\partial x} + \rho_4 g \frac{\partial z_B}{\partial x} + \rho_3 g \frac{\partial z_A}{\partial x} \tag{5.6c}$$

The differential of P_4 equals zero due to the layer being at rest. z_A and z_B do not depend on x, therefore, the differential is zero as well. This leaves,

$$\frac{\partial P_3}{\partial x} = g\left(\rho_4 - \rho_3\right) \frac{\partial h_3}{\partial x} \tag{5.7a}$$

Use the hydrostatic equation to find the differential of P_3.

$$\rho_3 f v_3 = g\left(\rho_4 - \rho_3\right) \frac{\partial h_3}{\partial x} \tag{5.8a}$$
$$v_3 = \frac{g\left(\rho_4 - \rho_3\right)}{\rho_3} \frac{1}{f} \frac{\partial h_3}{\partial x} \tag{5.8b}$$
$$v_3 = \frac{\gamma_3}{f} \frac{\partial h_3}{\partial x} \tag{5.8c}$$

Equivalently, u_3 can be found to be,

$$u_3 = -\frac{\gamma_3}{f} \frac{\partial h_3}{\partial y} \tag{5.9}$$

5.3 Slanted y_2

The form of the potential vorticity function $G_3(H)$ changes from $\frac{f_2}{H}$ to $a + \frac{b}{H}$. The values for a and b are determined using a polyfit through the potential vorticity against H for layer 3 of the slanted y_2 chosen.

Therefore, the heights of the layers are now,

$$h_3 = \frac{F}{G_3(H)} = f\frac{1}{a + \frac{b}{H}} = \frac{fH}{aH + b} \tag{5.10a}$$

$$h_2 = H - \frac{f}{G_3(H)} = \left(1 - \frac{f}{aH + b}\right) H \tag{5.10b}$$

This can be substituted into the equation for H to find,

$$H = \frac{(D_0^2(x,y) + H_0^2)^{\frac{1}{2}}}{\left[1 + \frac{\gamma_2}{\gamma_3}\left(1 - \frac{f}{aH+b}\right)\right]^{\frac{1}{2}}} \tag{5.11}$$

By moving the right side to the left, the equation equates to zero. Therefore, a minimisation technique can be used to solve for H.

5.4 North Pacific Ocean: Density layers and Outcrops

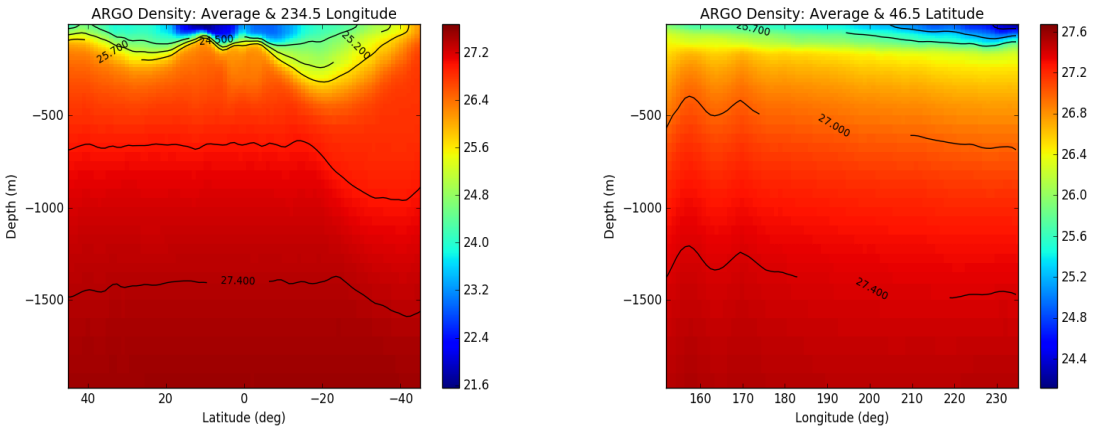

(a) Argo cross-section along the Eastern boundary

(b) Argo cross-section along y_w

Figure 5.1: The density layers chosen for the North Pacific Ocean found from the Argo data.

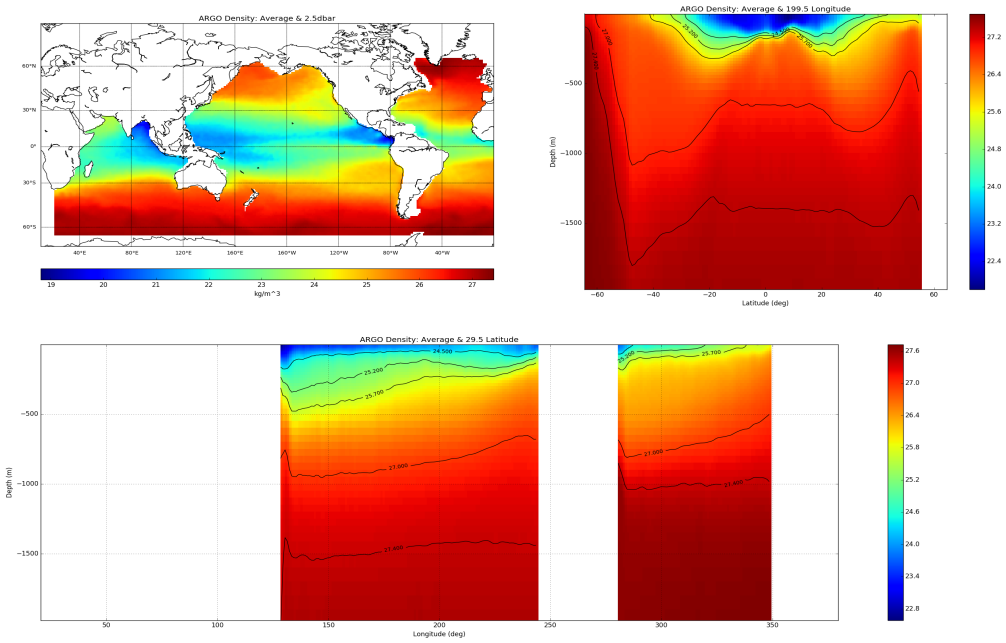

Figure 5.2: Density layers of the North Pacific Ocean for cross-sections 200° longitude and 30° latitude. The first graph shows the density at the surface of the ocean.

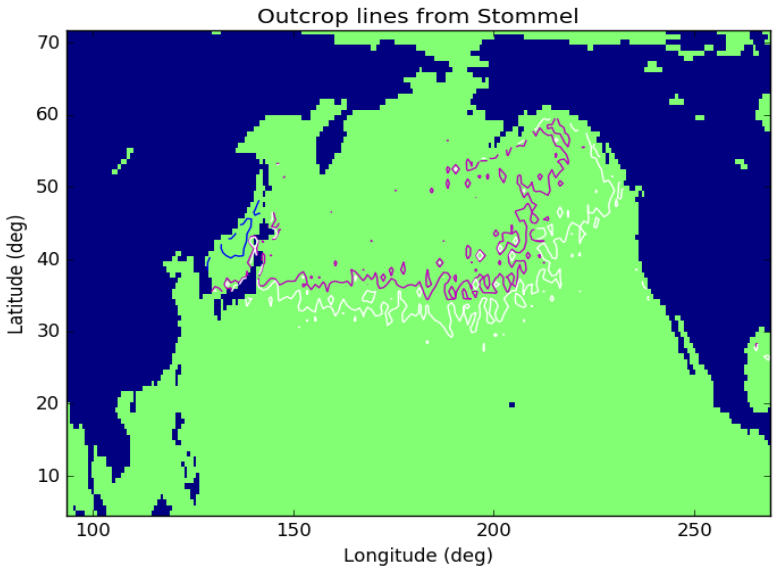

Figure 5.3: The outcrops calculated from Stommel's demon for the North Pacific. The y_3 (blue) line does not seem to visibly outcrop within this region. Therefore, y_3 does not outcrop before y_w so there is no conflict with the boundary conditions. This is a better fit compared to the North Atlantic Ocean. The y_2 and y_1 lines both curve up and east. This could not be modelled. The values chosen were 32° and 37° for y_1 and y_2, respectively.